Proceedings of the 2013 ASME Pressure Vessels and Piping Conference
PVP 2013
July 14-18, 2013, Paris, France

PVP2013-98059

SEVERE ACCIDENT CONDITION MODELING IN PWR ENVIRONMENT:CREEP RUPTURE MODELING

Frederick W. Brust
Engineering Mechanics Corporation of Columbus
Columbus, OH, USA

R. Iyengar, M. Benson
United States Nuclear Regulatory Commission
Rockville, MD, USA

Howard Rathbun
Lawrence Livermore National Laboratory
Livermore, CA, USA

ABSTRACT

A problem of interest in the nuclear power industry involves the response of pressurized water reactor (PWR) pressure boundary components under long-term station blackout (SBO) conditions. SBO is a particularly challenging event to nuclear safety, since all alternating current power required for core cooling is lost. If unmitigated, such a scenario will eventually lead to the reactor core being uncovered. Thermal-hydraulic (T-H), computational fluid dynamics, and structural combined creep/plasticity analyses of this scenario have been conducted and are presented here.

In this severe accident scenario, high temperatures can occur, and impart this thermal energy to the surrounding structures, including the reactor vessel, nozzles, reactor coolant system (RCS) hot leg piping and S/G tubes. At such high temperatures and pressures, creep rupture of RCS piping and/or steam generator (S/G) tubes becomes possible. The intent of this paper is to present a finite element based analysis model that can be used to evaluate the time to failure of the nozzle-weld-pipe configuration.

NOMENCLATURE

SBO	Station Black Out conditions
PWR	Primary Water Reactor
T-H	Thermal Hydraulic
RCS	Reactor Coolant System

INTRODUCTION

Advances in computational methods can facilitate the analysis of structures, systems and components under conditions within, and beyond-design basis. A specific problem of interest in the nuclear power industry involves the response of pressurized water reactor (PWR) pressure boundary components under long-term station blackout (SBO) conditions. SBO is a particularly challenging event to nuclear safety, since all alternating current power required for core cooling is lost. If unmitigated, such a scenario will eventually lead to the reactor core being uncovered. Thermal-hydraulic (T-H) and computational fluid dynamics analyses of this scenario have been conducted [1-3]. The results of these analyses indicate that, after several hours of SBO, a counter-current natural convection flow comprised of steam and hydrogen will form in the PWR hot leg, as shown in Figure 1 and Figure 2. The cold leg is assumed to be filled with sub-cooled reactor coolant, resulting in a loop seal. The PWR reactor coolant system (RCS) remains highly pressurized, relieved periodically by cycling of a power-operated relief valve. Once secondary-side inventory has been depleted in the steam generators (S/G), a condition known as "high-dry-low" is created, i.e. *high* RCS pressure, *dry* S/G secondary side, *low* S/G pressure.

In this severe accident scenario, the steam/hydrogen counter-current gas mixture will achieve high temperatures, and impart this thermal energy to the surrounding structures, including the reactor vessel, nozzles, RCS hot leg piping and S/G tubes. At such high temperatures and pressures, creep rupture of RCS piping and/or S/G tubes becomes possible. The intent of this paper is to present a finite element based analysis model that can be used to evaluate the time to failure of the nozzle-weld-pipe configuration. Many aspects of the model are simple approximations and serve as placeholders for future analysis inputs. Examples of these approximations include the linear heat flux magnitudes and visco-static boundary conditions. For future analyses, it is envisioned that these parameters would be adjusted to suit the needs of a particular problem. Accordingly, *the results presented in this article should not be interpreted to* *correspond to an actual accident scenario*; rather, they are merely illustrative of the types of results that can be obtained using this analysis procedure. This paper represents an extension to that in [4]. The results presented in this paper incorporate more accurate material properties with additional analyses..

NONLINEAR FINITE ELEMENT MODEL

The modeling process consisted of first obtaining the temperature time histories for an unlikely accident scenario termed the 'high-dry-low' conditions. This consists of high reactor coolant system pressure, dry steam generator side inventory, and low steam generator pressure and is illustrated in Figure 1. The red circled region shown in Figure 1 represents cross flow in the hot leg with hot gas persistent in the upper half of the pipe and cooler (but still hot) gas flowing in the bottom of the pipe in the opposite direction. Figure 2 provides an illustration of the temperature pattern produced.

Thermal Solution

The PWR RCS hot-leg finite element analysis is completed using the commercially available ABAQUS code [5] in a sequentially coupled thermal-visco-plastic fashion: the thermal analysis is completed to determine the temperature time history throughout the structure, and this result is mapped to a visco-static analysis to determine stress, strains and displacements. Figure 3 shows a cross-section view of the hot-leg geometry that includes a carbon steel nozzle clad with 316 stainless steel, a nickel-based Inconel weld, and a straight section of stainless steel pipe, along with the mesh refinement near the nozzle. The model geometry and dimensions are typical of a four-loop PWR.

For the thermal solution, heat flux is applied directly to the inner surfaces of the thermal finite element model. The analysis completed in [6] used a rather complex T-H calculation result heat flux vs. time traces. To simplify this portion of the analysis, a linear variation in heat flux vs. time is assumed. Figure 4 shows the linear heat flux vs. time applied to the inner surface of the top portion of the nozzle-weld-pipe model closest to the reactor vessel (i.e. the hottest portion of the model). The steam/hydrogen gas mixture loses heat energy as it travels along the top portion of the RCS hot leg toward the S/G. As an approximation, the heat flux in the middle third of the geometry is reduced by 12.5% as compared to the heat flux in the nozzle. The heat flux applied to the portion of the model furthest from the nozzle is reduced by 25%. As an approximation, the heat flux applied to the bottom portion of each pipe segment is 1/3 that of the corresponding top portion (Figure 4). While the above approximation scheme involves simple linear variations in heat flux with time, it accomplishes the goal for the task at hand, i.e. heat fluxes of appropriate magnitude are applied to six inner surface segments of the nozzle-weld-pipe model. Heat flux diminishes away from the nozzle and is lower on the bottom of the model than on the top. Future complex T-H results can be easily translated into this model. Figure 5 shows snap shots of the temperature at two different times after the start of the severe accident. It is clear the temperatures at the top are much higher than at the hot leg bottom due to the counter flow.

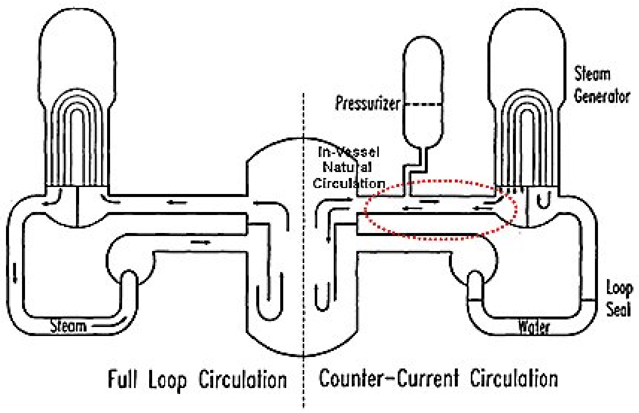

Figure 1 Natural circulation flow pattern in 'high-dry-low' conditions considered here

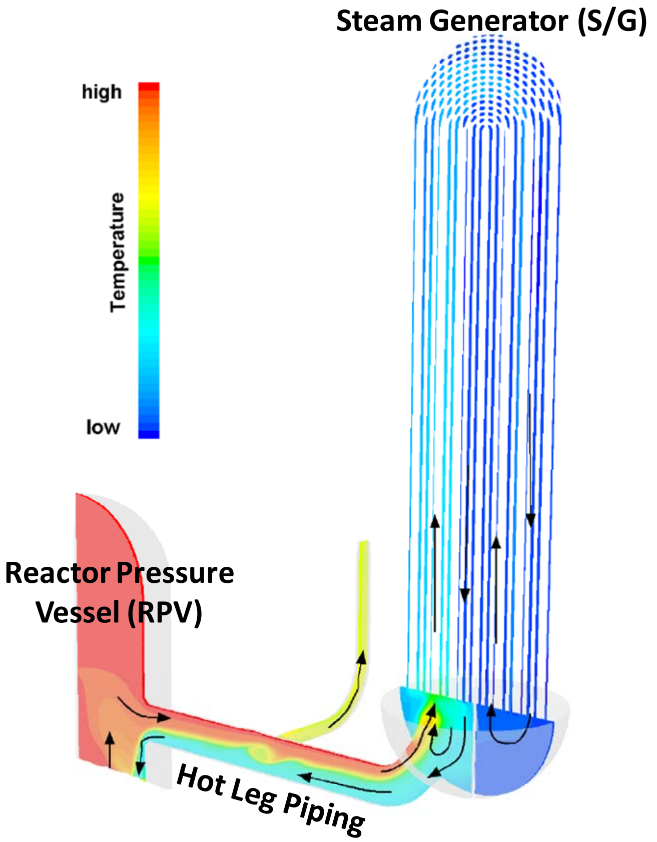

Figure 2 Natural circulation flow pattern temperature pattern

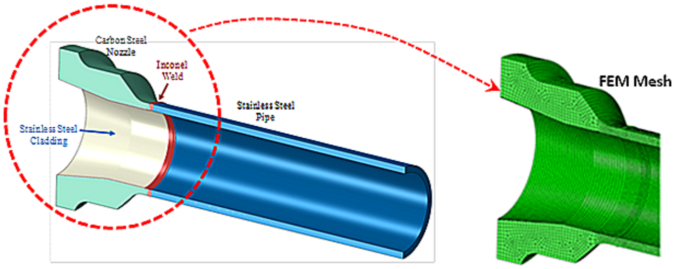
Carbon Steel Nozzle
Inconel Weld
Stainless Steel Pipe
Stainless Steel Cladding
FEM Mesh

Figure 3 Cross Section of RCS Hot Leg Analysis Model and mesh

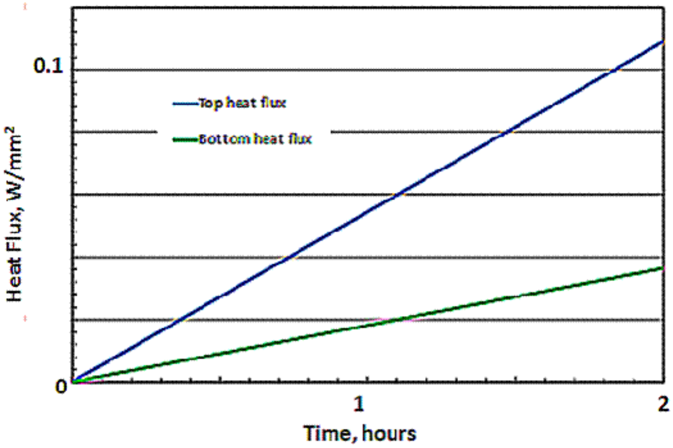

Figure 4 Linear Heat Flux vs. Time Applied to the Inner Surface of the Top and Bottom Portions of the Nozzle Region

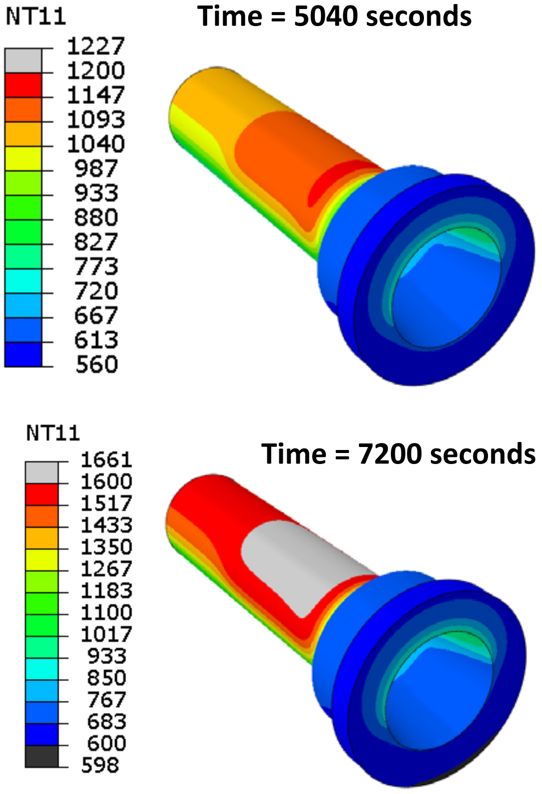
NT11
Time = 5040 seconds
1227
1200
1147
1093
1040
987
933
880
827
773
720
667
613
560
NT11
Time = 7200 seconds
1661
1600
1517
1433
1350
1267
1183
1100
1017
933
850
767
683
600
598

Figure 5 Temperature distribution in hot leg after severe accident start

Structural Solution

After completion of the thermal solution, the temperature time histories were input into the structural portion of the model. The first step of the analysis consisted of calculating the service operating loads which consist of gravity, pressure, and non-upset thermal loads. The second step consists of modeling the visco-plastic response of the system during the transient to determine likely failure and times and locations. The material model consisted of using a simple thermal plasticity combined with a secondary creep law. It is noted that, for future analyses, it may be more appropriate to use a continuum creep damage formulation (with or without coupling) in order to provide better failure predictions. The stress versus plastic strain curve used for the 316 stainless steel is shown in Figure 6. The properties used for the A508 carbon steel and the Alloy 182 weld metal can be found in [7] (including creep properties) and the elastic properties for the 316 SS can be found in [6]. Because material data was not available for temperatures higher than 1373 K these same properties were used at higher temperatures. However, as will be seen, failure is predicted before the temperatures get much higher than this.

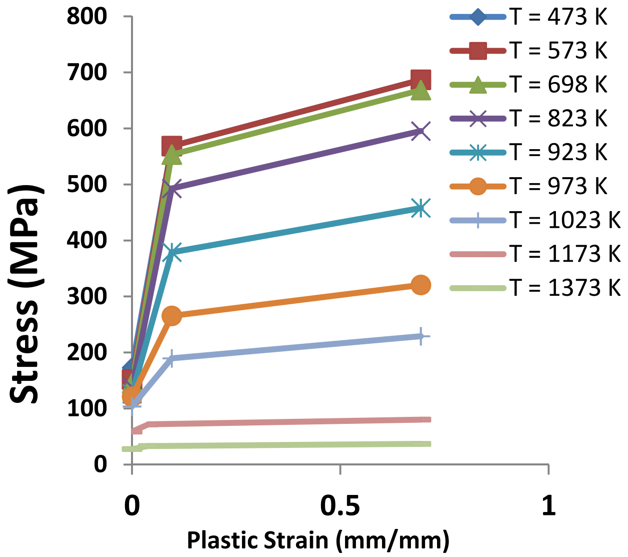

Figure 6 Temperature dependent stress strain curves for 316 stainless steel (from [6])

An ABAQUS power-law model is chosen to model creep behavior, given by:

$$\dot{\bar{\varepsilon}}^{cr} = A\tilde{q}^n t^m$$

where $\dot{\bar{\varepsilon}}^{cr}$ is the uniaxial equivalent creep strain rate, $\tilde{q}$ is the uniaxial equivalent deviatoric stress, and t is the total analysis time, and A, n are temperature dependent constants and m=0. The creep properties can be seen in Table 1 where stress is in MPa and time is seconds.

Table 1 Creep properties for 316 SS

A	m	T (K)
1.23E-43	4	294.1
1.62E-36	9.78	748
5.68E-36	9.97	773
1.15E-32	9.06	798
1.47E-29	8.2	823
1.02E-28	8.2	848
6.31E-28	8.2	873
4.49E-27	8.18	898
2.88E-26	8.16	923
5.68E-24	7.42	948
8.56E-22	6.72	973
3.34E-20	6.25	998
1.30E-18	5.77	1023
1.56E-17	5.89	1100
9.39E-17	5.85	1150
2.21E-15	5.85	1250
8.91E-15	5.85	1300
1.08E-15	5.85	1400

During the analysis a simple failure law based on the ASME Section III Subsection NH linear time fraction rule based on time spent at each temperature accumulated and normalized with Larson-Miller creep rupture data. In addition, a tensile plasticity failure strain of 4% will be used. This is not satisfactory, but will be used for initial assessments since this was used in Reference [1] and it is known that failure strains at high temperatures are quite small.

RESULTS

Time is assumed to begin several hours after SBO initiation, just as the RCS temperature begins to increase beyond normal operating conditions. The thermal analysis is allowed to run for a full two hours, while the visco-static analysis reaches a structural instability (excessive deformation) at approximately 5268 seconds after SBO start. For the thermal portion of the analysis, the outer surface of the model is treated as adiabatic, simulating insulated RCS piping. The initial temperature of all nodes is set to 550 K, corresponding to normal operating conditions. In the visco-static analysis, planar symmetry is assumed at both ends of the model. In addition, two nodes at the nozzle end are fixed to prevent rotational drift. A constant internal pressure of 15.2 MPa is applied to simulate RCS pressure.

Figure 7 shows the temperature distribution at the end of the visco-static analysis, corresponding to excessive deformation instability. While the inner-top surface of the nozzle is subject to the highest heat flux, the nozzle still remains at the lowest final temperature due to the large thermal mass. The top portion of the stainless steel pipe adjacent to the nozzle exhibits the greatest temperature increase, due to the relatively thin cross section, coupled with an applied heat flux that is larger than the right-most pipe section. Figure 8 shows the Mises equivalent stress evolution at times corresponding to 2183.5 seconds and 5268.5 seconds (at incipient failure). As seen in Figure 8, the portion of the model exhibiting the greatest deformation corresponds to the highest temperature region. However, the location of highest stress is the Inconel weld that connects the nozzle to the stainless steel pipe.

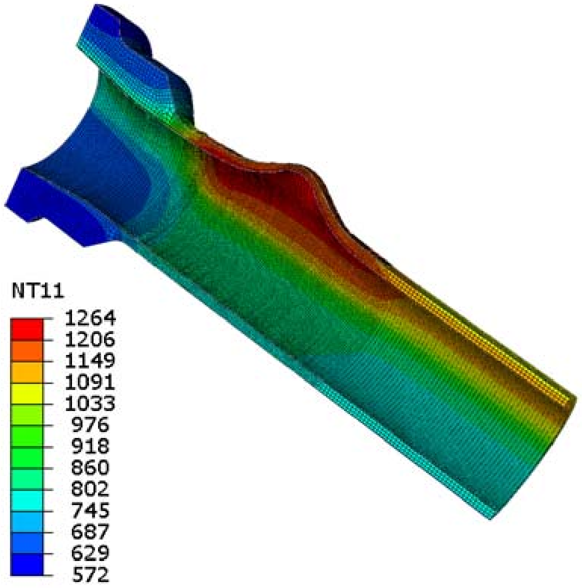

Figure 7 Nodal Temperatures at time = 5268 sec (degree K)

Figure 9 provides contour plots of equivalent plastic strain and equivalent creep strain, respectively, at the final viscostatic analysis increment. Clearly, the center of the bulged stainless steel piping experiences the greatest plastic and creep strain.

Based on the results presented here, there appear to be two potential points of failure in the structure:

1. the Inconel weld, because it has, by a large margin, the greatest Mises equivalent stress
2. the center of the bulged region, because it experiences the greatest equivalent plastic strain and equivalent creep strain

Note that, near failure, the creep behavior in the pipe adjacent to the nozzle has caused the stresses to relax significantly. However, at this high temperature, the yield stress is quite low (see Figure 6) so that appears that this is the region where failure may occur. While it is recognized that this constitutive law is not indicative of actual response under conditions where creep and plasticity occurs rapidly as during this severe accident modeling, these properties are all that is available at this time. Plans are to improve this model by using a creep-plasticity damage type model of the Spindler type in the future analyses.

To facilitate the failure analysis, Figure 10(a-c) shows, respectively, the Mises equivalent stress, equivalent creep strain, and equivalent plastic strain vs. time at the points identified above as potential failure locations. The top illustration shows both linear and nonlinear geometry results while the (b) and (c) are for nonlinear geometry only.

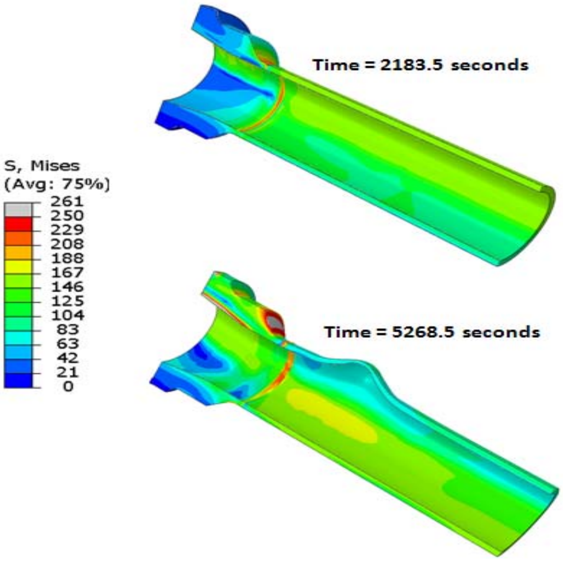
Time = 2183.5 seconds
S, Mises
(Avg: 75%)
261
250
229
208
188
167
146
125
104
83
63
42
21
0
Time = 5268.5 seconds

Figure 8 Mises Equivalent Stress at Time = 2183 and 5268 seconds

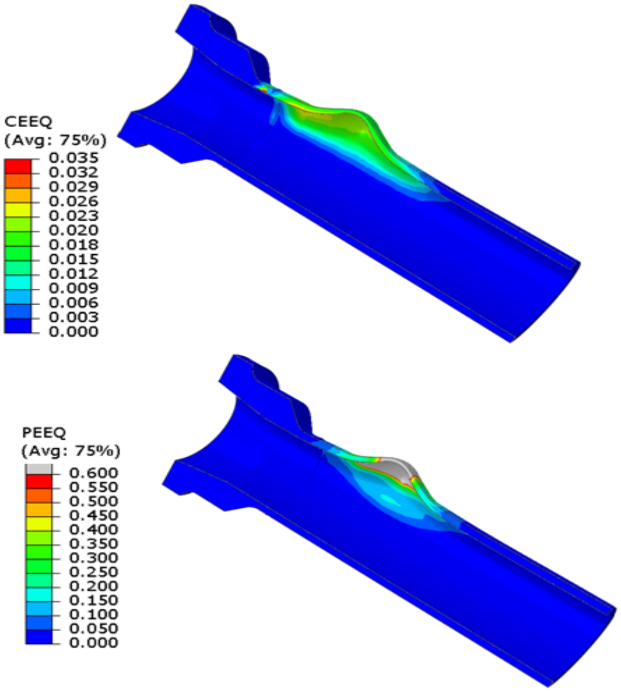
CEEQ
(Avg: 75%)
0.035
0.032
0.029
0.026
0.023
0.020
0.018
0.015
0.012
0.009
0.006
0.003
0.000
PEEQ
(Avg: 75%)
0.600
0.550
0.500
0.450
0.400
0.350
0.300
0.250
0.200
0.150
0.100
0.050
0.000

Figure 9 Equivalent Plastic Strain (bottom) and Creep Strain (top) at Time = 5268 seconds

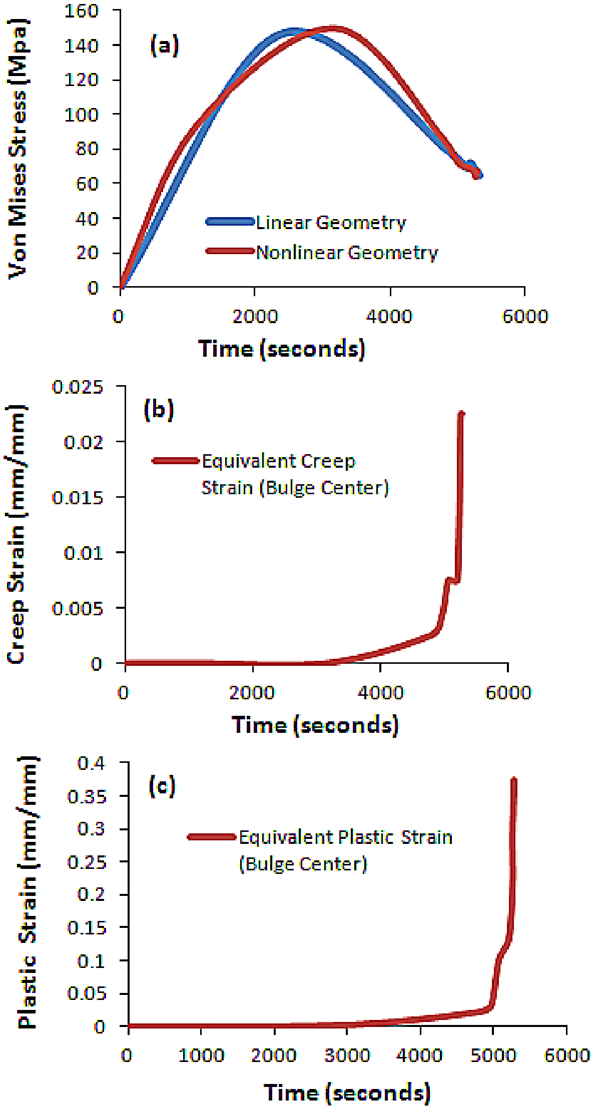

Figure 10 Mises stress (a), creep (b) and plastic (c) strains at center of bulge region in 316 SS pipe

FAILURE MODELS AND ANALYSIS

Two failure mechanisms are considered here: creep rupture and tensile instability. Creep rupture failure depends on both accumulations of creep strains along with the corresponding local constraint. A ductility damage exhaustion approach can be used for this (including the possibility of including the damage in the constitutive law where creep strain rates increase as damage develops which will be done in future analyses to better model the damage development). Tensile instability is net section collapse. It should be noted that the models applied here are associated with failure initiation, rather than failure of the overall structure, which would occur sometime later. Further, in the current analysis, the failure initiation models are applied at individual points. Future analyses will calculate damage for regions of interest, rather than isolated points.

Creep Rupture Failure.

Because creep ductility data were not available, we use the linear time fraction damage rule found in ASME code BPV III Section NH to determine to calculate the creep damage as follows:

$$\text{Creep Damage} = \sum \frac{\Delta t}{t_r(T,\sigma)}$$

,where Δt is the time interval at temperature T, σ is the von Mises effective stress, and t_r is the time to creep rupture at temperature T. Failure is predicted to occur when the creep damage is equal to 1. The Larson Miller parameter (LMP) was used to evaluate the time to rupture, t_r using the procedure suggested in the ASME code (section NH):

$$t_r = 10^{\left(\frac{LMP}{T}-C\right)}$$

where T is the absolute temperature in Kelvin, LMP is the Larson Miller parameter, which can be obtained approximately as a function of effective stress s as follows:

$$LMP = A * Log_{10}(\sigma) + B$$

and A, B, and C are material parameters (obtained from [6] and [8]). Tensile stress is required to develop creep cracks. Creep damage can also progress via void nucleation and growth, aided by hydrostatic stress states[1].

Tensile Damage.

Creep deformation tends to relax stresses in ‘displacement control’ situations (such as a thermal transient). Note that while there was a constant pressure of 15.2 MPa applied during the SBO incident, the large temperature gradients experienced due to the ‘high-dry’ condition (Figure 5 and Figure 7) between the top and bottom of the pipe adjacent to the weld produce a ‘displacement control’ type varying stress field. This creep relaxation can keep stresses below the yield strength of the material. However, creep deformation may not be fast enough to relax the stresses to below the yield stress. This can lead to tensile instability. Steel can accommodate about 4% strain at high temperatures prior to strain localization and plastic collapse (although this is a rough conservative estimate). Therefore, if through-thickness average tensile plastic strain reaches a value of 4% or more before creep rupture, the section is considered to have failed by tensile rupture.

As seen in Figure 10 the local plastic strain reaches 4% near 5000 seconds. Also, Figure 11 shows the accumulated creep damage in the center of the bulged region in the SS pipe adjacent to the weld. At the final analysis time, this region has not attained an accumulated creep damage value of 1. The apparent discrepancy between equivalent creep strain and creep damage will need to be investigated in further study. Indeed a more appropriate constitutive law is necessary to more appropriately model this response under SBO conditions where rapid creep and plastic damage can accumulate.

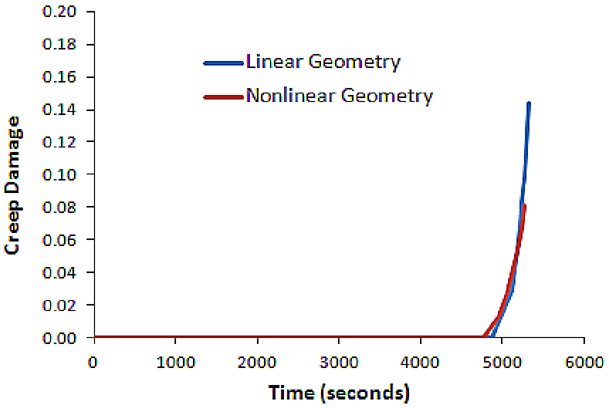

Figure 11 Creep damage Calculation at Center of Bulged Region

Collectively, Figure 9 through Figure 11 illustrate a procedure that can be used to assess time at failure initiation. Refinement of these models, particularly the strain criterion for tensile instability, is needed to obtain accurate predictions of failure initiation time. Further, once initiated, instability and/or crack propagation of the overall structure will need to be evaluated.

CONCLUSIONS

- Creep rupture and tensile instability failure initiation analysis, based upon parameters calculated by the finite element method, are applied to model nuclear piping under severe accident conditions.
- Predicted failure initiation time due to tensile instability can be calculated for a given strain criterion. The applicability of this model, and strain criterion values for the materials included in this study, remain for future work.
- Additional suggestions for further research include investigating alternative creep model constitutive relations, tensile failure criteria, implementing actual T-H analysis data as input, and reconciliation of creep damage and equivalent creep strain calculations.

ACKNOWLEDGMENTS

Dr. Christopher Boyd and Dr. Michael Salay of the U.S. NRC and Dr. Saurin Majumdar of Argonne National Laboratory are gratefully acknowledged for their helpful advice in this work. In addition, the authors thank Dr. Al Csontos of the US NRC for support of this work.

---

[1] Grain boundary sliding could also initiate cracks, aided by local shear stresses. Crack formation opens the possibility of growth by an elastic-plastic mechanism as well.

REFERENCES

[1] C.F. Boyd, “Prediction of Severe Accident Counter Current Natural Circulation Flows in the Hot Leg of a Pressurized Water Reactor” (U.S. Nuclear Regulatory Commission), Proceedings of ICONE 14, International Conference on Nuclear Engineering, 17-20 July 2006, Miami, Florida.

[2] U.S. Nuclear Regulatory Commission, “SCDAP/RELAP5 Thermal-Hydraulic Evaluations of the Potential for Containment Bypass During Extended Station Blackout Severe Accident Sequences in a Westinghouse Four-Loop PWR,” NUREG/CR-6995, July 2009.

[3] U.S. Nuclear Regulatory Commission, “Computational Fluid Dynamics Analysis of Natural Circulation Flows in a Pressurized-Water Reactor Loop under Severe Accident Conditions," NUREG-1922, March 2010.

[4] Rathbun, H., Benson, M. L., Iyengar, R., and Brust, F. W.., “Analysis of PWR Hot Leg in Severe Accident Conditions: Part I Creep Rupture Modeling”, Proceedings of Integrity of High Temperature Welds: Creep and Fatigue at Elevated Temperatures, 25-27 September, 2012, London, UK.

[5] ABAQUS User's Manual, Version 6.11, D'Assault-Systemes Simulia, 2011.

[6] Majumdar, S., Abou-Hanna, J., "Behavior of PWR Reactor Coolant System Components under Severe Accidents," Argonne National Laboratory report to US NRC.

[7] Brust, F. W., Zhang, T., Shim, D-J., Kalyanam, S., Wilkowski, G. M., Smith, M., and Goodfellow, A., “Summary of Weld Residual Stress Analyses for Dissimilar Metal Weld Nozzles”, Proceedings of ASME PVP conference, July 2010, Bellevue, WA, paper PVP2010-26106.

[8] API 579 “Fitness For Service”, June 5, 2007, Second Edition